NUMERICAL ANALYSIS OF TEST EMBANKMENT ON SOFT GROUND USING MULTI-LAMINATE TYPE MODEL WITH DESTRUCTURATION

M. CUDNY[1]

A multi-laminate constitutive model for soft soils incorporating structural anisotropy is presented. Stress induced anisotropy of strength, which is present in multi-laminate type constitutive models, is augmented by directionally distributed overconsolidation. The model is presented in the elastic-plastic version in order to simulate strength anisotropy of soft clayey soils and destructuration effects. Performance of the model is shown for some element tests and for the numerical simulation of a trial road embankment constructed on soft clays at Haarajoki, Finland. The numerical calculations are completed with the commercial finite element code capable to perform coupled static/consolidation analysis of soils. Problems related to the initiation of *in situ* stress state, conditions of preconsolidation, as well as difficulties linked to estimation of the model parameters are discussed. Despite simple assumptions concerning field conditions and non-viscous formulation of the constitutive model, the obtained final results are of a sufficient accuracy for geotechnical practice.

Key words: geomechanics, constitutive modelling, clays, multi-laminate, anisotropy, road embankment.

1. INTRODUCTION

The evidence of anisotropy of soft natural soils is shown in many high-quality laboratory studies for the stiffness and strength. The anisotropic mechanical characteristic of clayey soils originates from the arrangement of the clay fabric which is arisen during the sedimentation process. This arrangement is highly anisotropic for both natural and reconstituted clays. Most of the differences in the mechanical behaviour of natural and reconstituted soft soils are related to the existence of inter-particle bonds which are developed during the diagenesis of natural clays. The degree of anisotropy of the small-strain stiffness is of a similar intensity for both natural and reconstituted clays, however, the degree of the strength anisotropy is observed to be higher for natural material. Another important feature in the mechanical behaviour of the naturally bonded soils is a destructuration process, observed during plastic yielding. The destructuration process of a soft soil sample is connected with significant changes of its compressibility

---

[1] Department of Geotechnics, Geology and Maritime Engineering, Faculty of Civil and Environmental Engineering, Gdańsk University of Technology, Gdańsk, Poland. e-mail: mcud@pg.gda.pl

and the strength anisotropy. An exemplary experimental evidence is given by Leroueil [1].

The presented version of the model for soft natural clays is developed to model realistically the strength anisotropy and its evolution, as well as destructuration effects, especially on the so-called *wet side* of the critical state, where hardening takes place. The extension to the multi-laminate framework of modelling by Pietruszczak and Pande [2] is used where it is proposed to model the inherent anisotropy of the strength by introducing the directional dependency of the material parameters. This approach is found to be straightforward and intuitive for the modelling of strength cross-anisotropy and volumetric destructuration of soft clay. Only a few additional parameters to the standard material constants are used for this task. The model is presented in the basic version – open for any extensions. Its key feature is the introduction of a spatially distributed anisotropic overconsolidation. In the model, overconsolidation is directly related to the degree of bonding of soil fabric. For this reason, the characteristic mechanical process of destructuration of natural soft soils is combined with changes of strength anisotropy.

In 1997 the Finnish National Road Administration organised an international competition for calculating and predicting the behaviour of the road embankment at Haarajoki. The embankment was founded on soft soil deposits which are typical for the region, FinnRA [3]. These deposits are characterised by a high degree of anisotropy and natural inter-particle bonding. The embankment was constructed in 1997, and the competition is already closed. Nevertheless, the available data concerning the general *in situ* behaviour of the embankment and results of the associated laboratory tests are very useful for the validation of different modelling methods. The results of some finite element analyses are already published in the literature, e.g. Aalto [4] and Yildiz [5]. The scope of the presented analysis is not to compete with other modelling approaches but to validate and investigate possibilities of the proposed multi-laminate constitutive model.

2. Formulation of the model

The most important and the original features of the model are presented. The detailed description of the multi-laminate framework may be found in Pande and Sharma [6] or Pietruszczak and Pande [7]. In the multi-laminate framework, soil is assumed to be a solid block behaving elastically (*macro level*), intersected by an infinite number of randomly oriented planes where plastic straining may occur (*micro level*). A static constraints are used. This means, that the actual *macro* stress tensor σ is projected to the *micro* stress vectors $\bar{\sigma}^k$ on every k-th plane where the possible plastic strain increments are calculated. Components of $\bar{\sigma}^k$ are defined in the local coordinate system where the third unit vector is aligned with the normal to the k-th sampling plane $\mathbf{n}^k$. Plastic contribution from all planes are then spatially summed up in order to obtain

the macro plastic strain increment: $d\bar{\varepsilon}^{pk} \overset{\Sigma}{\rightarrow} d\varepsilon^p$. In the numerical implementation, this summation from an infinite number of planes, is evaluated by using a numerical integration rule with a finite m number of sampling planes:

$$(2.1) \quad \begin{aligned} &\text{stress projection}: \bar{\sigma}_i^k = T_{ij}^{\sigma k}\bar{\sigma}_j, \quad i = 1..3,\ j = 1..6 \\ &\text{plastic micro strain increment}: d\bar{\varepsilon}_i^{pk} = d\lambda^k \frac{\partial g^k}{\partial \bar{\sigma}_i^k}, \quad i = 1..3 \\ &\text{plastic macro strain increment}: d\bar{\varepsilon}_i^p = \sum_{k=1}^{m} T_{ij}^{\varepsilon k}\bar{\varepsilon}_j^{pk} w_k, \quad i = 1..6,\ j = 1..3 \end{aligned} \quad ,$$

where w_k are the weights, $d\lambda^k$ and g^k are the plastic multiplier and potential function on the k-th plane respectively. $\mathbf{T}^{\sigma k}$, $\mathbf{T}^{\varepsilon k}$ are the stress and strain transformation matrices respectively. Note that the macro stress and strain tensors are expressed here exceptionally in the vector form: $\bar{\sigma}$, $\bar{\varepsilon}^p$. Among various integration schemes proposed by Fliege and Maier [8], the system with 64 sampling planes is used.

2.1. Elastic part

In the multi-laminate framework the elastic part of the strain increment $d\varepsilon^e$ is calculated on the macro level. A broad class of elastic models for soils may be used, depending on the significance of the small elastic deformations in the simulated engineering problem.

This paper is focused on the modelling of the evolution of compressional strength anisotropy where stress dependency of the elastic stiffness is of a special importance. The coupling of anisotropy and stress dependency of elastic stiffness is, however, complex and requires additional, not standard material parameters. For these reasons the isotropic hypoelastic stiffness based on Hooke's law, often used in the critical state models, is applied with a constant Poisson ratio v and a pressure dependent Young modulus defined as $E(p) = 3(1 - 2v)p/\kappa^*$, where κ^* is the swelling index estimated from $\ln p$-ε_v compression diagrams.

2.2. Yield surface and plastic potential on the micro level

The constitutive law is isotropic within the micro sampling plane, and the yield function may be expressed as a function of the normal and shear invariants of micro stress vector:

$$(2.2) \qquad \sigma_n^k = -\bar{\sigma}_3^k, \quad \tau^k = \sqrt{\left(\bar{\sigma}_1^k\right)^2 + \left(\bar{\sigma}_2^k\right)^2}.$$

The simplicity of the constitutive relationship is favourable, since the performance of the multi-laminate model is validated on the macro level after spatial integration.

Multi-laminate framework in elastoplasticity is limited in its description of post-peak or softening behaviour. This fact is connected with the static constraints that are used.

In structured soft natural clays, shear softening may occur, e.g. for undrained stress paths starting from stress states in the overconsolidated region. However, the shear softening has a discontinuous nature – irreversible strains localise in a narrow shear band and the surrounding material is unloaded. The modelling requires some additional techniques related to the regularisation if the material model is to be implemented into a finite element code.

Because of this limitation, the conservative solution is chosen. In the model, the shear strength in the overconsolidated area is controlled by the Mohr-Coulomb criterion, and it is not a subject to hardening or softening.

The yield surface on the sampling plane level is shown in Fig. 1. It consists of the *cone* and *cap* parts which are responsible for the shear and compressional strength respectively.
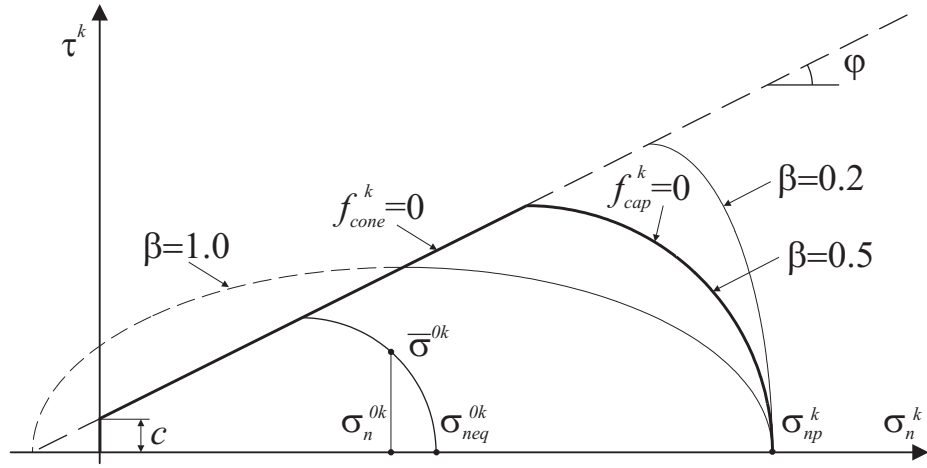

Fig. 1. Yield surface on the sampling plane level.
Rys. 1. Powierzchnia plastyczności w układzie pojedynczej płaszczyzny w modelu wielopłaszczyznowym

The cone part uses a non-associated flow rule, and the yield function and plastic potential are:

$$(2.3) \qquad f_{cone}^k = \tau^k - \sigma_n^k \mu - c = 0, \; g_{cone}^k = \tau^k - \sigma_n^k \tan\psi,$$

where $\mu = \tan\varphi$ and φ, c, ψ are the effective friction angle, effective cohesion and dilatancy angle respectively. The incorporation of c is optional, however, in finite element computations, a small value is chosen in order to avoid a singular apex of the yield surface.

The cap part of the yield surface uses an associated flow rule and the yield function is defined as

$$(2.4) \quad f_{cap}^k = \left(\sigma_n^k - \sigma_{np}^k\right)\mu^2 \left[\frac{2\beta c}{\mu} + (1+\beta)\,\sigma_{np}^k + (-1+\beta)\,\sigma_{np}^k\right] + \left(\tau^k \beta\right)^2 (1+\beta) = 0,$$

where σ_{np}^{k} is a micro preconsolidation pressure and β is an additional parameter which controls the steepness of the cap surface. On the macro level, β allows to control the asymptotic value of K_0^{nc} resulting from the simulation of an oedometer compression.

2.3. DIRECTIONAL OVERCONSOLIDATION

Pietruszczak and Pande [2] have shown the improved version of the multi-laminate framework where the anisotropic distribution of mechanical properties is obtained with a help of microstructure tensor. They proposed that the strength parameters like the friction angle or cohesion may be distributed directionally. However, as it is found in the present study, for materials like soft natural clays it would be more realistic to distribute the overconsolidation ratio which is directly related to the initial bonding of the soil fabric. In order to agree with the critical state mechanics of clayey soils, strength parameters are taken as intrinsic constants; Burland [9].

The microstructure tensor **a** is defined as a measure of material fabric (spatial arrangement of clay platelets or inter-granular contacts). For practical applications, it appears to be difficult to obtain any information related to the microstructure, since advanced methods of the fabric analysis are very complicated and they are not standardised. Nevertheless, for structure related directional distribution, only a deviatoric measure of the material microstructure **Ω** is needed. This tensor is traceless ($\Omega_{kk}=0$) and symmetric. In the case of cross-anisotropy, typical for natural soft soil deposits, there are two distinct eigenvalues of **Ω**. In the geometrical frame of principal axes of cross-anisotropic microstructure (x_2 vertical), tensor **Ω** has the following components:

$$(2.5) \qquad \Omega_{ij} = 0 \text{ for } i \neq j, \quad \Omega_{11} = \Omega_{33} = -\Omega_v/2, \quad \Omega_{22} = \Omega_v.$$

Note that only one parameter identifying the spatial bias of cross-anisotropic microstructure (Ω_v) is needed which may be estimated on the basis of mechanical behaviour observed in laboratory tests.

The initial distribution of the preconsolidation pressure on every k-th sampling plane can be expressed by the following equation:

$$\sigma_{np}^{k} = \sigma_{neq}^{0k}\left(1 + b_0^k\right), \quad b_0^k = b_0\left(1 + \Omega_{ij}n_in_j\right) = b_0\left[1 - \frac{\Omega_v}{2}\left(1 - 3\left(n_2^k\right)^2\right)\right];$$

$$(2.6) \qquad \sigma_{neq}^{0k} = \frac{\sigma_n^{0k} - \frac{\beta}{\mu}\left[-c + \sqrt{\left(c + \sigma_n^{0k}\mu\right)^2 + \left(-1 + \beta^2\right)\left(\tau^{0k}\right)^2}\right]}{1 - \beta}, \quad \text{or}$$

$$\sigma_{neq}^{ok} = \sigma_n^{0k} + \frac{\left(\tau^{0k}\right)^2}{\mu\left(c + \sigma_n^{0k}\mu\right)}, \quad \text{for} \quad \beta = 1.0$$

where b_0 is an average or isotropic bonding parameter. Now, the stress induced strength anisotropy (related to the initial stress state σ^0) is amplified and adjusted by the com-

ponent which is connected with the microstructural bonding. Initialisation of the directional overconsolidation in the presented model is shown schematically, with the help of polar plots, in Fig. 2.
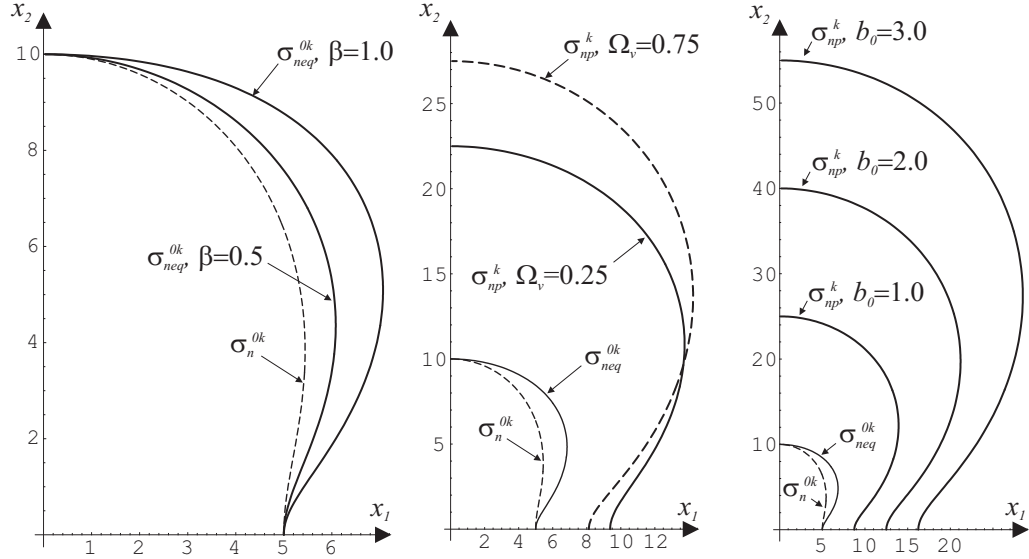

Fig. 2. Polar distribution of the initial overconsolidation. Left to right: influence of the parameter β; effects of the parameter Ω_v; different degrees of bonding b_0; (distributions are shown for an example triaxial initial stress state: $\sigma_{22}^0 = -10$ kPa, $K_0 = 0.5$, scales concern the units of stress).

Rys. 2. Rozkład kierunkowy początkowej prekonsolidacji. Od lewej do prawej: wpływ parametru β; wpływ parametru Ω_v; różne stopnie cementacji b_0; (rozkłady pokazano przy wybranym osiowo symetrycznym stanie naprężenia: $\sigma_{22}^0 = -10$ kPa, $K_0 = 0.5$, skale dotyczą jednostek naprężenia)

2.4. Hardening law

Incorporation of the destructuration process is achieved through the evolution equation for the state variable, representing bonding on every sampling plane b^k. The modelling framework proposed by Gens and Nova [10] is used. In this framework hardening or softening is influenced by two competing components. The first of which is related to the evolution of the so-called unbonded yield surface, usually hardening, whereas the second is connected with the shrinking of the yield locus due to bond degradation.

The evolution equation for b^k, which controls the bonded yield locus, is defined as

$$(2.7) \qquad b^k = b_0^k \exp\left(-a\left|\varepsilon_n^{pk}\right|\right),$$

where a is an additional parameter describing the reduction of bonding with increasing accumulated normal plastic strain ε_n^{pk}.

The standard law from the Cam-clay model for normally consolidated soils, is employed for the unbonded component of hardening. The final hardening law for the preconsolidation pressure on the k-th sampling plane may be written in the incremental form as

$$(2.8) \qquad d\sigma_{np}^k = \sigma_{np}^k \left[\frac{1}{\lambda^* - \kappa^*} - \frac{ab_0^k \exp\left(-a\left|\varepsilon_n^{pk}\right|\right)}{1 + b_0^k \exp\left(-a\left|\varepsilon_n^{pk}\right|\right)} \right] d\varepsilon_n^{pk},$$

where λ^* is a compression index estimated from $\ln p$-ε_v compression diagrams.

Depending on the chosen values of parameters, both volumetric hardening or softening may result. Volumetric softening is indeed realistic for some heavily structured soils but it may be difficult to control in the implementation algorithm. By inspecting the hardening law, it can be derived that for fixed values of the parameters λ^*, κ^* and b_0^k, the condition of no volumetric softening implies

$$(2.9) \qquad a \le a_{\max}^k = \frac{1 + b_0^k}{b_0^k \left(\lambda^* - \kappa^*\right)}.$$

It is found that instead of adopting a as the model parameter it is better to impose the ratio $a_r = a/a_{max}^k$. This means that the value of a is also a subject to the directional distribution, and consequently the superscript k is used: $a^k = a_r a_{max}^k$.

3. Element tests

The presented multi-laminate model for soft soils is implemented into the commercial finite element code *Plaxis* within the user defined soil model facility, Brinkgreve [11]. Performance of the model is shown for three types of element tests. Namely oedometer compression, triaxial undrained compression/extension, and triaxial radial stress path tests. For more detailed element studies and validations, as well as implementation aspects, the reader is refered to Cudny and Vermeer [12]. The following reference set of the material parameters are used:

$$(3.1) \qquad \begin{aligned} \varphi &= 30°, \ c = 0\text{kPa}, \psi = 0°, \ \upsilon = 0.2, \ \kappa^* = 0.02, \ \lambda^* = 0.1, \ \beta = 0.75; \\ b_0 &= 1.0, \ a_r = 1.0, \ \Omega_v = 0.5 \end{aligned}$$

Note that the first line in Eq. (3.1) represents standard parameters which may be classified as the intrinsic parameters, and the second line represents parameters related to the description of the initial state of the material bonding. The choice of the initial *in situ* stress state has also an important influence on the simulated material behaviour,

since in the multi-laminate models for clay this affects directly the stress-induced anisotropy of the strength. For element tests, the initial *in situ* stress state is chosen as

$$(3.2) \qquad \sigma_{22}^0 = -45\text{kPa}, \ \sigma_{11}^0 = \sigma_{33}^0 = K_0^{nc}\sigma_{22}^0 = -22.5\text{kPa}, \ \Rightarrow p_0 = 30\text{kPa}.$$

3.1. Oedometer compression

The evidence of the destructuration phenomenon is well recognisable during the constant rate of strain oedometer compression tests. The intensity of the destructuration is proportional to the value of the parameter b_0 (see Fig. 3). In the laboratory, during the oedometer compression test, the stress ratio after the destructuration phase is asymptotically approaching an unique value of K_0^{nc}. In the model, this can be controlled by the parameter β, like it is presented in Fig. 3.
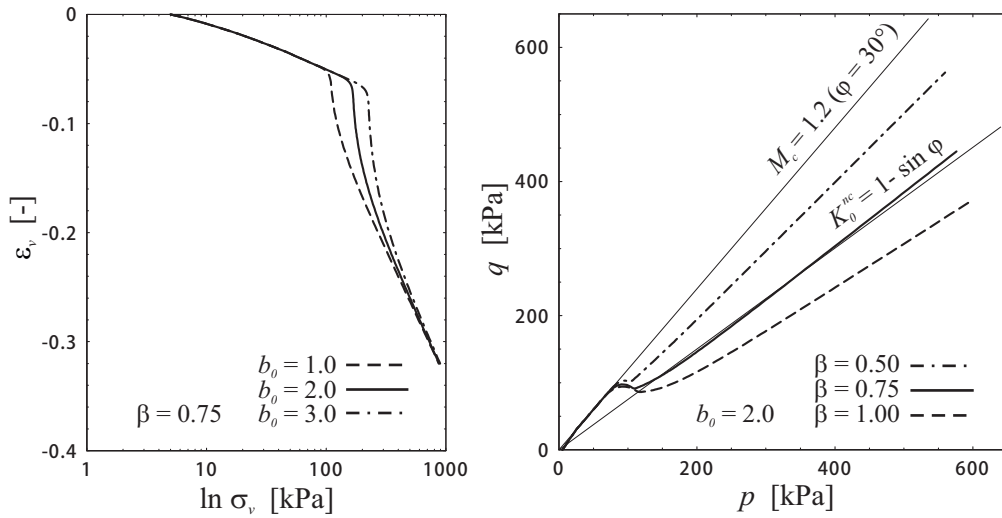

Fig. 3. Influence of the parameters b_0 and β on the simulated behaviour in the oedometer compression.
Rys. 3. Wpływ parametrów b_0 i β w symulacji zachowania się gruntu w warunkach edometrycznych

3.2. Undrained triaxial compression and extension

Undrained triaxial compression and extension tests are simulated for different levels of destructuration. The results of these simulations are shown in Fig. 4. Before undrained triaxial compression or extension phases, the material is anisotropically consolidated along the K_0^{nc}-line to the five stress states (a-e).

The tests (a) start from the K_0^{nc}-stress state where no sampling planes are mobilised and hence the behaviour is typical for the lightly overconsolidated clays excluding a
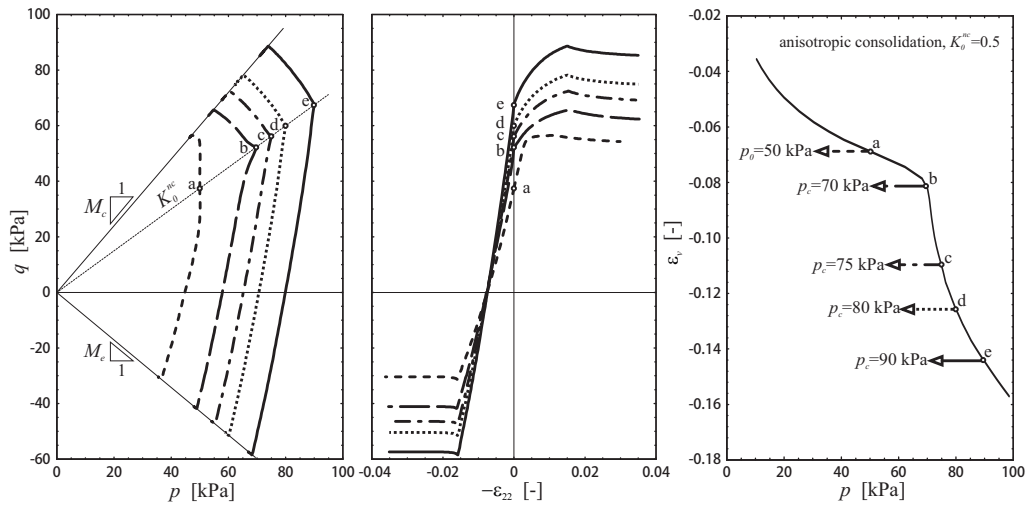
Fig. 4. Simulations of the undrained triaxial compression and extension tests for different levels of destructuration along the K_0^{nc}-line.

Rys. 4. Symulacja ściskania i rozciągania w aparacie trójosiowym w różnych fazach destrukturyzacji wzdłuż linii K_0^{nc}

softening phase. The tests (b) start from the point where the rate of the bonding reduction is very high and the bulk stiffness is almost equal to zero. This contractive tendency provides a fast increase of the excess pore water pressure and the resulting stress paths for compression and extension form a characteristic sharp *nose* on the $p - q$ plane. This phenomenon is still apparent for the tests (c) where the intensity of destructuration is still high but it disappears gradually for the higher consolidation stresses (d-e).

When the shear strength is reached on some sampling planes, there are still a number of planes where micro stresses remain on the cap yield surface with a strong tendency to contract. The effects are, hence, similar to the application of negative value for the dilatancy angle, and softening-like behaviour is observed.

3.3. Macro yield surface from radial stress path tests

Radial stress path tests in triaxial apparatus are usually performed to obtain the shape and size of the yield surface for a given loading rate. In the multi-laminate models, it is not possible to obtain the macro yield surface explicitly, as yielding on the macro level is not distinct, and relates to the integrated behaviour from the micro level. The yielding develops progressively, and the same techniques for capturing the yield point have to be applied for simulation and experimental results. The commonly used methods of the location of volumetric yield point by line extrapolations are not perfect, nevertheless,

it is the only mean to study the development of the macro yield surface resulting from the multi-laminate model.

The obtained macro yield surfaces on the $p - q$ plane are presented in Fig. 5. In order to obtain the presented graphs, initial conditions in the multi-laminate model are imposed or induced by loading at the beginning. Then, the radial stress path tests are simulated starting from the small isotropic stress state (p_0=5 kPa). Twelve radial stress paths are applied for every macro yield locus on the $p - q$ plane: two directions parallel to the compression (M_c) and extension (M_e) shear failure lines, $\eta=q/p$=1.2 and η=-0.857 respectively; ten radial directions from η=-0.8 to η=1.0 with an interval of 0.2.

The left-hand graph in Fig. 5 presents the evolution of the yield locus for different levels of destructuration. Destructuration is induced by loading along the K_{nc}^0-line, similarly as in the consolidation phase for the undrained triaxial simulations (Fig. 4). The shape of the intact yield surface transforms with increasing levels of destructuration to the shape characteristic for the stress induced anisotropy. The rate of this process is related to the degree of bonding, as well as the value of structural cross-anisotropy parameter Ω_v. The right hand side graph displays the influence of the parameter Ω_v on the shape of the intact yield surface. Asymmetry about the p-axis, as well as steepness of the yield surface, is proportional to the value of the parameter Ω_v.
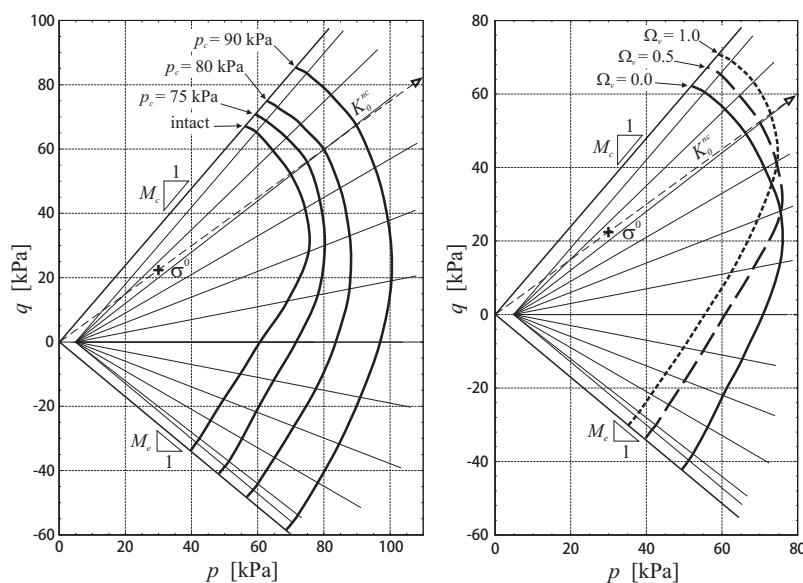

Fig. 5. Evolution of the macro yield surface for different levels of destructuration and its initial shape for different degrees of cross-anisotropy Ω_v.
Rys. 5. Zmiany powierzchni plastyczności w skali makro w różnych fazach destrukturyzacji oraz początkowy kształt tej powierzchni przy różnych wartościach stopnia anizotropii (transwersalnej izotropii) Ω_v

4. Embankment and ground conditions

The longitudinal and cross sections of the Haarajoki test embankment are shown schematically in Fig. 6. The embankment is 3 m high and 100 m long. The width at the top is 8 m. In the longitudinal direction of the embankment half of the soft ground deposits are improved by the installation of vertical drains. A geotextile reinforcement is applied at the bottom of the embankment. In the current study only the part of the embankment without ground improvement (cross section 35840) is analysed.
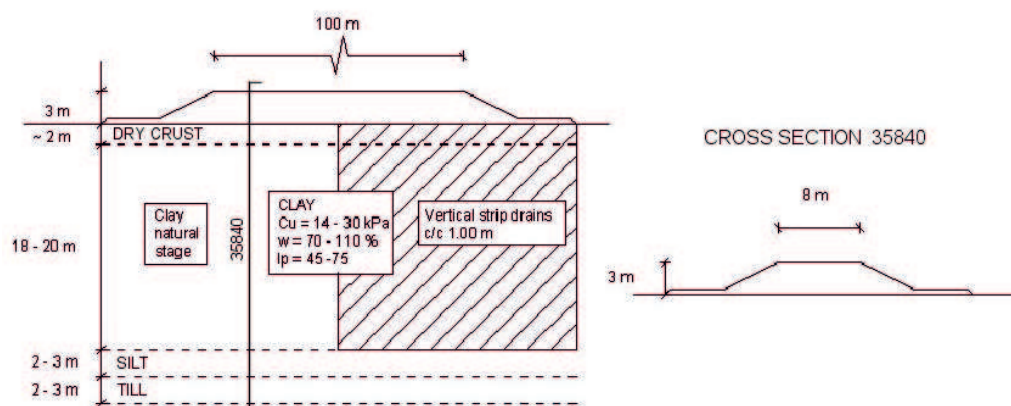

Fig. 6. Longitudinal and cross sections of the Haarajoki test embankment. Cross section 35840, where no vertical drains were applied, is analysed.
Rys. 6. Przekrój podłużny próbnego nasypu drogowego w Haarajoki. Analizę numeryczną przeprowadzono w przekroju poprzecznym 35840, gdzie nie zastosowano pionowych drenów

The construction of the embankment is executed in 0.5 m high stages using a gravel fill with a density of 21 kN/m^3. The construction is completed within 3 weeks.

The ground water table is located at surface level, and excess pore pressures of -3 to -10 kPa were measured in the deposit before the construction started. The soft ground consists of a shallow 2 m thick layer of highly overconsolidated crust laying over a 20 m thick soft soil deposit. The most compressible soil layers are located at depth between 2 and 10 m.

5. Initial conditions and material parameters

Instead of refining ground layers by different values of material parameters, the main soft soil deposit is simulated with the same *intrinsic* constants. Only the initial values of the state variables representing bonding and overconsolidation varies with depth. Intrinsic parameters are estimated on the basis of available laboratory tests results and

parameter sets previously used in other calculation studies. Throughout the paper all stress quantities are effective.

The soft soil deposit at Haarajoki can be classified as a *fat* clay with a content of clay size particles higher than 50%. The organic content is between 1.4 and 2.2%. The water content varies between 67 and 112% and is often higher than the liquid limit. This observations, together with the measured high sensitivity of the clay (up to 50), demonstrate an important mechanical evidence of a fragile inter-particle bonding.

Indeed, results of constant rate of strain (CRS) oedometer compression tests clearly display a destructuration process characteristic for Scandinavian soft clays. Some oedometer compression curves given in the records from the Haarajoki competition materials are shown in Fig. 7. The degree of bonding, directly linked with the intensity of destructuration, decreases slowly with depth. However, the degree of bonding appears to be quite high and constant for the shallow layers up to a depth of 5 m. It is important to note that an intrinsic compression index λ^*, defined as the final inclination of compression curves in semi-logarithmic plots, is approximately constant for all layers.
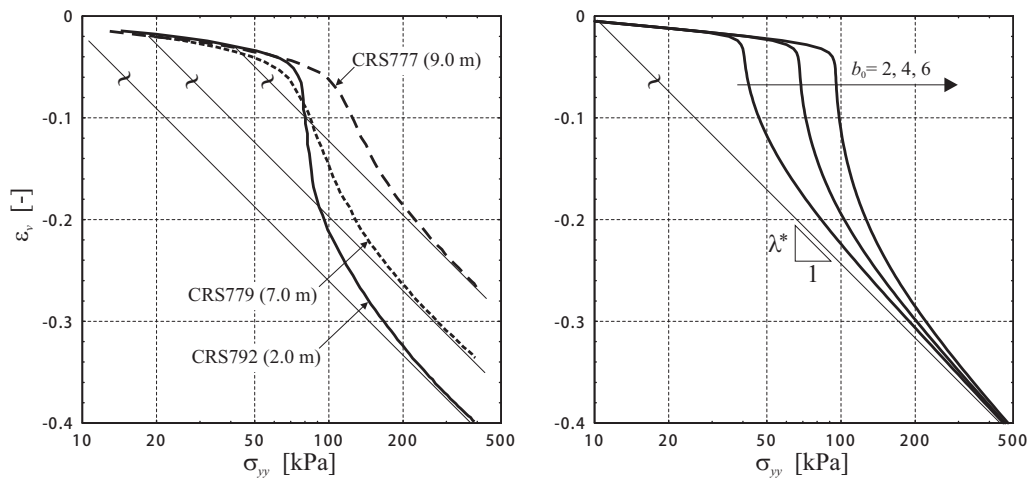

Fig. 7. Left: Results of CRS oedometer compression tests on the soft clay from Haarajoki; Right: Influence of the parameter b0 on the simulated behaviour during oedometer compression.
Rys. 7. Wyniki ściskania edometrycznego przy stałej prędkości odkształcenia (CRS) słabonośnego iłu z Haarajoki (strona lewa); Wpływ parametru b0 w symulacji zachowania się tego gruntu podczas ściskania edometrycznego (strona prawa)

In the applied multi-laminate model, the parameter of initial bonding is imposed separately on every sampling plane, and for the cross-anisotropic sediments this

distribution is defined as

$$(5.1) \qquad b_0^k = b_0 \left(1 + \Omega_{ij} n_i n_j\right) = b_0 \left[1 - \frac{\Omega_v}{2}\left(1 - 3\left(n_2^k\right)^2\right)\right].$$

This implies the following maximal and minimal values of preconsolidation pressure on the sampling planes with the respective normal directions oriented vertically and horizontally:

(5.2)

$$\max\left(\sigma_{np}^k\right) = \sigma_{neq}^{0k}\left[1 + b_0\left(1 + \Omega_v\right)\right] = \sigma_{np}^v, \quad \min\left(\sigma_{np}^k\right) = \sigma_{neq}^{0k}\left[1 + b_0\left(1 - \frac{\Omega_v}{2}\right)\right] = \sigma_{np}^h.$$

Estimation of the parameter b_0 can be carried out by back-calculations of oedometer tests or directly from isotropic compression tests, like it is shown in Cudny and Vermeer [12]. The influence of the parameter b_0 on the shape of compression curves is depicted in Fig. 7.

Another important problem, when imposing initial conditions, is the proper initiation of the directionally dependent preconsolidation pressure. It should be noted that the preconsolidation pressure on the horizontal sampling planes can not be equated to the traditional preconsolidation pressure from oedometer tests, as yielding observed on the macro level is an integrated plastic behaviour from the sampling planes and occurs progressively. Having estimated the value of b_0 and the initial *in situ* stress state σ^0, i.e. σ_{yy}^0 and K_0, it can be found that the direct use of the distribution from Eq. (2.6) results in much higher preconsolidation than this measured or assumed. This happens especially in heavily structured soils. It follows that for the initiation of directional overconsolidation, a reduced stress level σ^{0*} should be applied by keeping the same value of K_0.

In the analysis, first the distributions of the mean preconsolidation stress p_p, bonding b_0 and K_0 with depth are set, as it is shown in Fig. 8. Then, in every integration point, the reduced mean stress p_0^* and related stress components, needed for directional distribution, are calculated as

$$(5.3) \qquad p_0^* = \frac{p_p}{1 + b_0} \Rightarrow \sigma_{yy}^{0*} = \sigma_n^{0v*} = \sigma_{neq}^{0v} = \frac{3p_0^*}{1 + 2K_0}, \sigma_{xx}^{0*} = \sigma_n^{0h*} = \sigma_{neq}^{0h} = K_0\sigma_{yy}^{0*}.$$

In Eq. (5.3) superscripts v and h are linked with vertical (y) and horizontal (x) directions normal to the sampling planes respectively. Results of the applied procedure are shown in Fig. 9.

The parameter Ω_v controls the degree of the strength cross-anisotropy in the model. This parameter has an influence on the shape of macro yield surface which results from the multi-laminate model. Its influence is also visible when simulating oedometer compression tests on the vertically and horizontally trimmed samples, see Cudny and
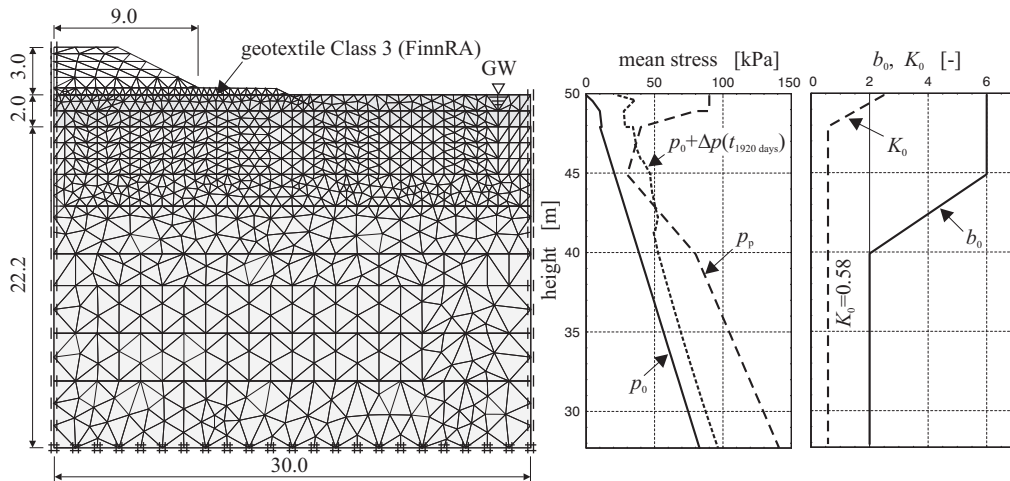
Fig. 8. Finite element discretisation of the boundary problem and initial distributions of p_p, K_0 and b_0.
Rys. 8. Dyskretyzacja na elementy skończone w rozwiązywanym zagadnieniu brzegowym oraz przyjęte
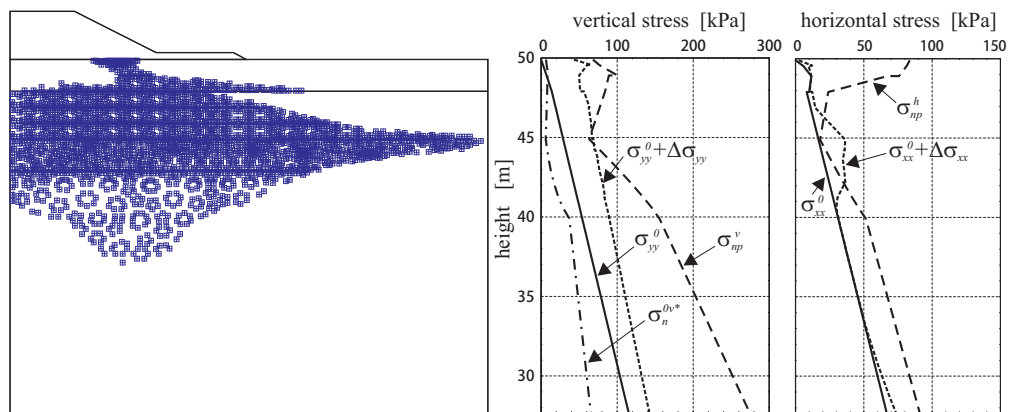początkowe rozkłady wartości p_p, K_0 i b_0

Fig. 9. Volumetric yielding points in multi-laminate model and distribution of stress at the centre line.
Rys. 9. Punkty w których doszło do akumulacji objętościowego odkształcenia plastycznego w modelu
wielopłaszczyznowym (multi-laminate) oraz rozkład naprężenia wzdłuż osi nasypu

Vermeer [12]. Nevertheless, it seems to be impossible to estimate it on the basis of a single standard laboratory test. It is found that choosing values close to the K_0–value brings satisfactory results for soft natural soils. Values of remaining material parameters used in the analysis are listed in Table 1.

Table 1

Values of the material parameters.
Wartości parametrów materiałowych

Layer	Depth m	γ kN/m^3	φ deg	c kPa	ψ deg	ν –	κ^* –	λ^* –	β –	Ω_v –	a_r –	k_x m/d	k_y m/d
embank.*	–	21	35	3.0	0	0.15	–	–	–	–	–	3.0	1.0
crust	0-2	17	29	7.7	0	0.2	0.004	0.070	0.84	0.6	1.0	6.5e-3	6.5e-3
soft soil	2-22	15	25	5.7	0	0.2	0.012	0.111	0.95	0.6	1.0	7.0e-4	4.5e-4
*) Mohr-Coulomb model is used for embankment material; additional parameter: E=50000 kPa													

6. ANALYSIS AND RESULTS

Simulations of the Haarajoki test embankment behaviour is completed with the same 2D finite element code used previously for element tests.

All calculation phases including 6-stages construction of the embankment and consolidation for the period of 1920 days (~5.3 years) are computed as fully coupled static/consolidation analysis. User defined soil model facility is used both for the implementation of the constitutive law, as well as for imposing the initial stress and the preconsolidation conditions.

The finite element discretisation of the boundary problem is shown in Fig. 8. 1847 of 6-noded **u**-p plane strain elements are used. Measured and calculated vertical displacements are compared at the centre line and at the points located 4 and 9 m from the centre line. Horizontal displacements are compared along the vertical profile located 9 m from the centre line.

These comparisons between field measurements and simulation results are presented in Fig. 10 and Fig. 11. The results obtained for the first set of material parameters and initial conditions are only satisfactory for the vertical displacements. The horizontal deformation is generally overestimated. After small corrections to the depth distribution of the preconsolidation pressure (increased), very good results are obtained for the vertical displacements, but the horizontal displacements are still overestimated.

Differences between the measured and simulated horizontal displacements have already occurred in the early construction phase of the emebankment. However, their absolute values have not changed much in the course of consolidation. This would suggest that sources of inaccuracy are linked with the applied isotropic elasticity in the model. The unsound influence of elastic isotropy may be important in the shallow layer of dry crust, where the largest stress changes take place.

measurements: centre line (CL) □,   4 m from CL left ▽,   right ○,   9 m from CL left ×,   right +
simulations: CL ⎯⎯⎯ ,   4 m from CL ⎯ · ⎯ · ,   9 m from CL ⎯ ⎯ ⎯
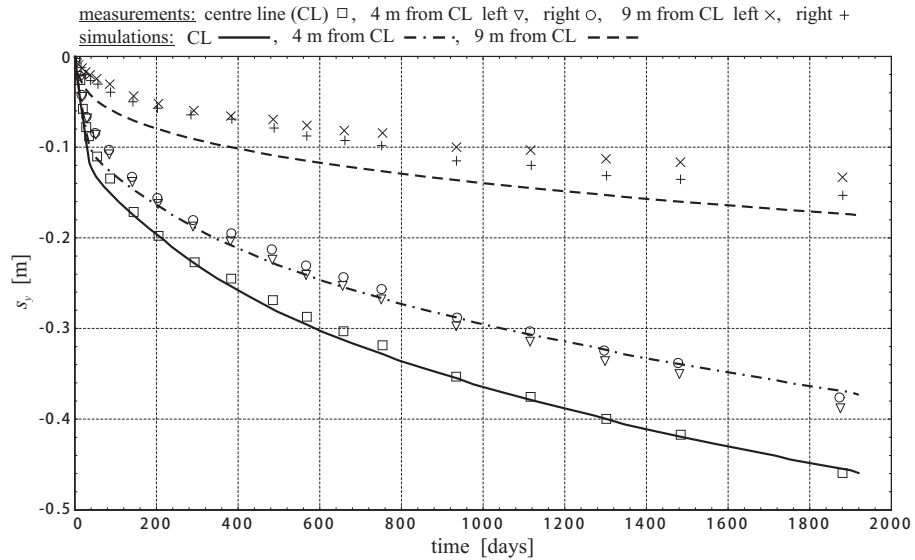

Fig. 10. Measured and simulated time-settlement curves for points located at the embankment base.
Rys. 10. Krzywe osiadania w czasie wybranych punktów w podstawie nasypu uzyskane z pomiarów oraz
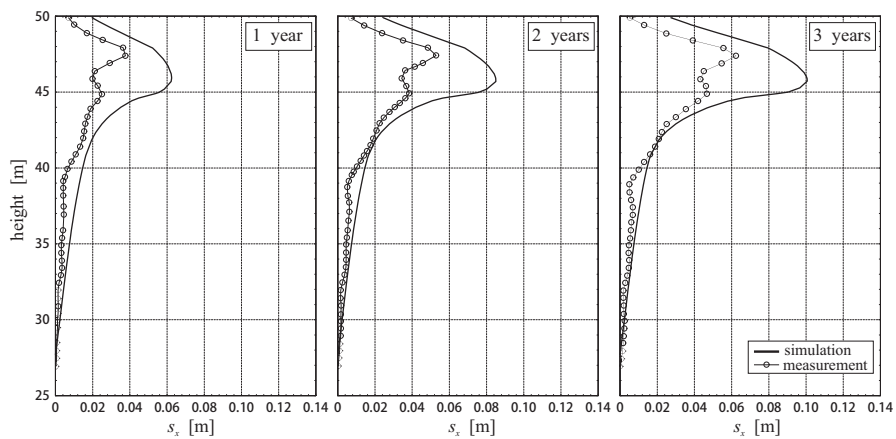obliczeń

Fig. 11. Comparison between measured and simulated horizontal displacements (s_x) and their
development during the consolidation for the vertical profile located at the embankment toe.
Rys. 11. Porównanie zmian rozkładów składowej poziomej przemieszczenia (s_x) w czasie, w pionowym
profilu zlokalizowanym w dolnej krawędź nasypu, na podstawie wyników pomiarów oraz obliczeń

On the other hand, taking into account the assumed simplicity of the initial field conditions and use of average intrinsic parameters for a quite deep deposit of soft clays, the final accuracy of the simulations is satisfactory.

7. Conclusions

The multi-laminate model for soft soils incorporating bonding anisotropy and destructuration is presented in the version which is potentially simple using the framework of rate independent plasticity. The basic idea applied in the formulation of the model is the directional distribution of the overconsolidation or bonding over the sampling planes in the multi-laminate framework, and to connect this distribution with the microstructure of the soil. Microstructure is understood here as the arrangement of the clay fabric and interparticle bonds having influence on the strength anisotropy.

The results of element simulations with this model are shown in order to give realistic results according to the known experimental evidence. The model is useful especially for the geotechnical problems where compression of natural soft clays has an important contribution in the general behaviour.

Important extensions like introduction of the rate-dependency and elastic anisotropy may be applied, however, with a cost of additional material parameters.

The behaviour of test road embankment founded on the soft clays deposit at Haarajoki, Finland is simulated with finite element method. The developed multi-laminate constitutive model is calibrated and used for this task giving results which are close to the field observations.

8. Acknowledgement

References

1. S. Leroueil, F. Tavenas, F. Brucy, P. La Rochelle, R. Marius, *Behavior of destructured natural clays*, Journal of the Geotechnical Engineering Division, ASCE 105(GT6): 759-778, 1979.
2. S. Pietruszczak, G.N. Pande, *Description of soil anisotropy based on multi-laminate framework, Short communication*, International Journal for Numerical and Analytical Methods in Geomechanics **25**, 195-208, 2001.
3. Finnish National Road Administration, Competition to calculate settlements at the Haarajoki test embankment. *Competition programme, Competition Materials*. FinnRA, 1997.

4. A. AALTO, R. REKKONEN, M. LOJANDER, *The calculations on Haarajoki test embankment with the finite element program Plaxis 6.31.* [In:] A. Cividini (ed.), Proc. 4th Europ. Conf. on Numerical Metchods in Geotechnical Engineering NUMGE98, Udine: 37-46, Springer, 1998.

5. A. YILDIZ, M. KARSTUNEN, H. KRENN, *Effect of Anisotropy and Destructuration on Behavior of Haarajoki Test Embankment*, International Journal of Geomechanics, ASCE. **9**(4), 153-168, 2009.

6. G.N. PANDE, K.G. SHARMA, *Multi-laminate model of clays – a numerical evaluation of the influence of rotation of the principal stress axes.* International Journal for Numerical and Analytical Methods in Geomechanics **7**, 397-418, 1983.

7. S. PIETRUSZCZAK, G.N. PANDE, *Multi-laminate framework of soil models – plasticity formulation.* International Journal for Numerical and Analytical Methods in Geomechanics **11**, 651-658, 1987.

8. J. FLIEGE, U. MAIER, *A Two-Stage Approach for Computing Cubature Formulae for the Sphere.* Ergebnisberichte Angewandte Mathematik, Universität Dortmund 139T, 1996;
http://www.personal.soton.ac.uk/jf1w07/nodes/nodes.html.

9. J.B. BURLAND, *On the compressibility and shear strength of natural clays, 30th Rankine lecture.* Géotechnique **40**(3), 329-378, 1990.

10. A. GENS, R. NOVA, *Conceptual bases for a constitutive model for bonded soils and weak rocks.* [In:] A. Anagnostopoulos, F. Schlosser, N. Kalteziotis & R. Frank (ed.), *Geotechnical Engineering of Hard Soils – Soft Rocks*, Proc. IS-Athens'93: 485-494, Rotterdam: Balkema, 1993.

11. R.B.J. BRINKGREVE, *Plaxis finite element code for soil and rock analyses, Version 8.* Lisse: Balkema, 2002.

12. M. CUDNY, P.A. VERMEER, *On the modelling of anisotropy and destructuration of soft clays within the multi-laminate framework.* Computers and Geotechnics **31**, 1-22, 2004.

ANALIZA NUMERYCZNA NASYPU DROGOWEGO POSADOWIONEGO NA GRUNCIE
SŁABONOŚNYM Z ZASTOSOWANIEM MODELU WIELOPŁASZCZYZNOWEGO
Z DESTRUKTURYZACJĄ

S t r e s z c z e n i e

W artykule przedstawiono model wielopłaszczyznowy (multi-laminate) uwzgledniający anizotropię struktury słabonośnych gruntów drobnoziarnistych. Anizotropia indukowana naprężeniem, którą otrzymuje się przy zastosowaniu modeli wielopłaszczyznowych, jest dodatkowo wzmocniona poprzez wprowadzone prekonsolidacji zależnej od orientacji przestrzennej. Model przedstawiono w wersji sprężysto-plastycznej, w której możliwa jest symulacja anizotropii wytrzymałości słabonośnych gruntów drobnoziarnistych oraz zjawiska destrukturyzacji. Działanie modelu pokazano w symulacjach numerycznych wybranych badań elementarnych oraz przy zastosowaniu w modelowaniu numerycznym odkształcenia słabonośnego podłoża gruntowego pod próbnym nasypem drogowym w Haarajoki, Finlandia. Symulację numeryczną przeprowadzono przy użyciu komercyjnego programu metody elementów skończonych pozwalającego na analizę sprzężonych zagadnień brzegowych statyki i konsolidacji. Omówiono zagadnienia związane z przyjęciem warunków początkowych stanu naprężenia *in situ* oraz warunków prekonsolidacji, jak również przedstawiono problemy związane z przyjęciem parametrów modelu. Pomimo przyjęcia prostych zasad dotyczących warunków początkowych oraz przy pominięciu efektów lepkości w modelu konstytutywnym, otrzymane wyniki pozwoliły na osiągnięcie wystarczającej w praktyce geotechnicznej dokładności w stosunku do wartości pomierzonych.